Exfoliated Nanocomposite from Polyaniline Graft Copolymer/Clay

Woo Jin Bae, Keon Hyeong Kim, and Won Ho Jo*

Hyperstructured Organic Materials Research Center and School of Materials Science and Engineering, Seoul National University, Seoul 151-742, Korea

Yun Heum Park

School of Applied Chemistry and Chemical Engineering, Sungkyunkwan University, Suwon 440-746, Korea

Received June 14, 2004; Revised Manuscript Received October 5, 2004

ABSTRACT: Exfoliated polyaniline (PANI)/clay nanocomposites were prepared by in-situ polymerization of aniline onto pre-exfoliated water-soluble poly(styrenesulfonic acid-*co*-aminostyrene) (P(SSA-*co*-AMS))/clay nanocomposite or by simple blending of poly(styrenesulfonic acid-*g*-aniline) (PSSA-*g*-PANI) with clay. When an aqueous mixture of P(SSA-*co*-AMS) and clay was treated with 1 M HCl (aq), clay layers are exfoliated into the polymer matrix due to the electrostatic interaction between the positive charge of nitrogen (NH_3^+) in P(SSA-*co*-AMS) and the negatively charged surface of clay layers. The electrical conductivity of the nanocomposite is slightly lower than that of pure PSSA-*g*-PANI, but the thermal stability and coatability of the nanocomposite become better compared with PSSA-*g*-PANI.

Introduction

Conducting polymers have become a popular basic material for advanced applications such as electrode,[1] static electricity dissipation,[2] and metal anticorrosion and marine-fouling prevention.[3,4] Polyaniline (PANI) is one of the most technologically important materials because of its environmental stability in a conducting form, easiness and low cost of synthesis, unique redox properties,[5] and high conductivity.[6] However, the physical properties of PANI are not satisfactory for practical applications. In this regard, PANI/clay nanocomposite may open a way to construct novel organic−inorganic hybrid systems showing electrical conductivity as well as good physical properties.[7]

Several methods to prepare PANI/clay nanocomposite have been reported. One commonly used method to prepare the nanocomposite is intercalation of aniline into the gallery of clay layers followed by in-situ polymerization.[8−13] Emulsion polymerization is also used for preparation of PANI/clay nanocomposite,[14,15] where the emulsifier in the emulsion system contributes to maximization of the affinity between hydrophilic host (clay) and hydrophobic guest (aniline).

Although many studies on PANI/clay nanocomposites have been carried out as mentioned above, they obtained the intercalative structure. Since exfoliated nanocomposites have better physical properties such as stiffness, strength, and barrier property with far less inorganic content than intercalative nanocomposites, it is rationalized that the higher the degree of exfoliation in polymer/clay nanocomposites, the greater the enhancement of these properties. Recently, it has been reported that PANI/clay nanocomposites with exfoliated silicate layers are successfully prepared using an organically modified clay.[16] However, the method for the organophilic modification of clay is so complicated that the process for preparation of nanocomposite is less economical.

* To whom correspondence should be addressed. Phone: +82-2-880-7192. Fax: +82-2-885-1748. E-mail: whjpoly@plaza.snu.ac.kr.

In our previous study[17] we successfully synthesized a novel conducting PANI graft copolymer, poly(styrenesulfonic acid-*g*-aniline) (PSSA-*g*-PANI), which is soluble in both water and polar organic solvent. Since the PSSA-*g*-PANI copolymer is soluble in water, it is likely expected that the graft copolymer could be homogeneously mixed with silicate layers dispersed in water, and as a result the PANI/clay nanocomposite with exfoliated structure could be prepared. Here, we report that an exfoliated PANI/clay nanocomposite without organophilic modification of Na^+−MMT is first prepared using both in-situ polymerization and simple blending of water-soluble PSSA-*g*-PANI with Na^+-MMT.

Experimental Section

Preparation of in-Situ PSSA-*g*-PANI/clay Nanocomposite. Poly(sodium styrenesulfonate-*co*-*tert*-butoxycarbonyl-aminostyrene) (P(SSNa-*co*-BOC-AMS)) was synthesized by copolymerization of sodium styrenesulfonate (SSNa) and *tert*-butoxycarbonyl-aminostyrene (BOC-AMS).[17] Na^+−MMT (Closite Na^+: Southern Clay Products Inc.; water content < 2.0 wt %, aspect ratio = 100−1000) (0.15 g) and P(SSNa-*co*-BOC-AMS) (0.8 g) were dissolved in 30 mL of 1 M HCl aqueous solution and then sonicated for 3 h using an ultrasonic generator for swelling of the Na^+−MMT. The swelling procedure under acidic conditions not only helps a polymer chain to penetrate into the gallery of clay layers but also eliminates the BOC groups from P(SSNa-*co*-BOC-AMS) to yield P(SSA-*co*-AMS).

For graft copolymerization of aniline (ANI) onto P(SSA-*co*-AMS) in P(SSA-*co*-AMS)/Na^+−MMT solution, ANI (0.2 g) was first added to the solution for 0.5 h during stirring, and then 20 mL of ammonium persulfate (0.49 g)/1 M HCl aqueous solution was dropwise added to the solution at 0 °C to yield PSSA-*g*-PANI/Na^+−MMT. After 6 h of reaction a dark green solution was obtained and further purified by dialysis using a semipermeable membrane (molecular weight cutoff, 3500) to remove low molecular weight compounds. The resulting solution was concentrated and precipitated into acetone. The precipitate was filtered and dried under vacuum at 60 °C for 24 h. Elemental analysis shows that the PANI content in PSSA-*g*-PANI/clay nanocomposite is 56 mol %. The chemical structures of polymers used in this work are represented in Figure 1.

Simple Blending of PSSA-*g*-PANI and Clay. Na^+−MMT (0.15 g) and PSSA-*g*-PANI (1.0 g; the PANI content, 54 mol

10.1021/ma048829b CCC: $27.50
Published on Web 11/20/2004

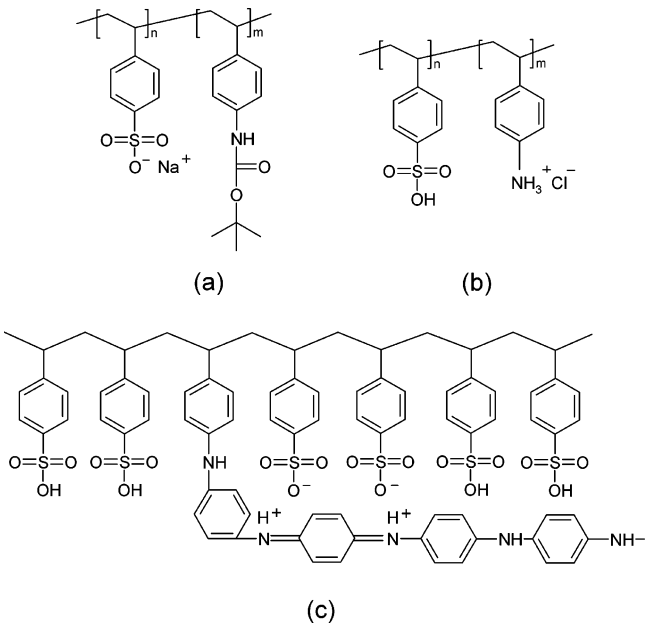

Figure 1. Chemical structures for (a) P(SSNa-*co*-BOC-AMS), (b) P(SSA-*co*-AMS), and (c) PSSA-*g*-PANI.

%) were dissolved in deionized water and then sonicated for 3 h using an ultrasonic generator for swelling of the Na^+−MMT. The solution was concentrated and precipitated into acetone. The precipitate was filtered and dried under vacuum at 60 °C for 24 h.

Characterization. The change in basal spacing of the nanocomposites was measured using an X-ray diffractometer (MAC Science, MXP 18XHF) with Ni-filtered Cu Kα radiation (λ = 0.1542 nm; 40 KV; 30 mA). Transmission electron microscopy (TEM) (JEOL-200CX) was used with an acceleration voltage of 120 kV. The samples for TEM were prepared by evaporation of a drop of diluted aqueous solution of in-situ composite or simple blending of PSSA-*g*-PANI and clay onto a 200 mesh copper grid. FT-IR spectra were recorded on a Perkin-Elmer FT-IR 1725X spectrometer, and UV−vis spectra of PSSA-*g*-PANI/clay nanocomposite were obtained using a Perkin-Elmer UV/VIS/NIR spectrophotometer (Lambda-6). The electrical conductivity of PSSA-*g*-PANI/clay nanocomposite was measured in a compressed pellet (1.5 cm diameter × 0.05 cm thick) at room temperature by the four-probe technique using an electrometer. Details for measuring electrical conductivity have been described in an earlier paper.[18] Thermogravimetric analysis (TGA) was carried out at a heating rate of 10 °C/min under nitrogen atmosphere. The surface morphologies of PSSA-*g*-PANI and PSSA-*g*-PANI/clay nanocomposite film as spin coated on silicon wafer were observed using a field emission scanning electron microscope (FESEM) (JSM-6630F).

Results and Discussion

As the BOC group is removed from P(SSNa-*co*-BOC-AMS) in P(SSNa-*co*-BOC-AMS)/clay nanocomposite to yield P(SSA-*co*-AMS), a new peak is observed at 2623 cm^{-1} due to NH_3^+ stretching vibration, as can be seen in Figure 2a and b. This new peak at 2623 cm^{-1} disappears when aniline (ANI) is graft polymerized onto P(SSA-*co*-AMS) in P(SSA-*co*-AMS)/clay solution, indicating that PANI is successfully grafted onto P(SSA-*co*-AMS). When the FTIR spectrum of in-situ PSSA-*g*-PANI/clay nanocomposite (Figure 2c) is compared with that of simple blending of PSSA-*g*-PANI and clay (Figure 2d), it is realized that the two spectra are identical, indicating that the PSSA-*g*-PANI in in-situ composite has the same chemical structure as the PSSA-*g*-PANI in the simple blending and has all the characteristic peaks of PSSA-*g*-PANI and clay. This provides evidence that PANI is successfully in-situ grafted onto P(SSA-*co*-AMS) in the P(SSA-*co*-AMS)/clay solution, considering that PANI homopolymer is not soluble in water. Characteristic peaks of doped PANI are observed at 1563, 1474, 1303, 1230, 804, and 518 cm^{-1}, corresponding to δ_{N-H} (quinoid ring structure), δ_{N-H} (benzenoid ring structure), ν_{C-N}, ν_{C-N}^+, δ_{C-H}, and δ_{N-H} (out-of-plane bending), respectively, and characteristic peaks of Na^+−MMT are also observed at 1036 and 465 cm^{-1} (ν_{Si-O} and δ_{Si-O}), as shown in Figure 2c.

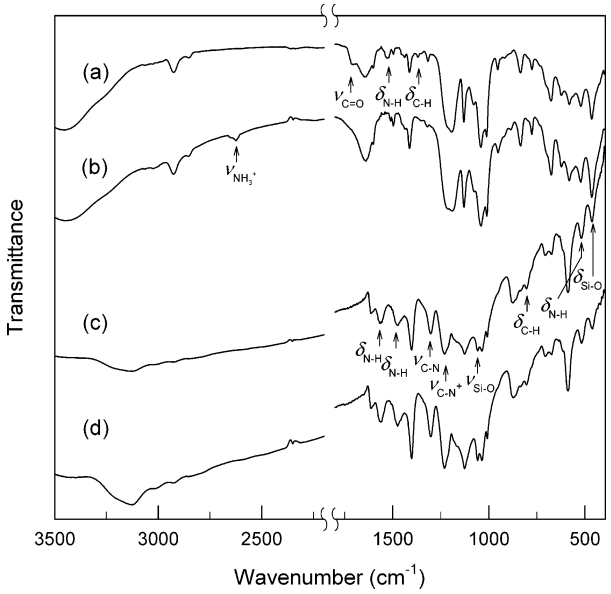

Figure 2. FTIR spectra of (a) P(SSNa-*co*-BOC-AMS)/clay nanocomposite, (b) P(SSA-*co*-AMS)/clay nanocomposite, (c) in-situ PSSA-*g*-PANI/clay nanocomposite, and (d) simple blending of PSSA-*g*-PANI and clay.

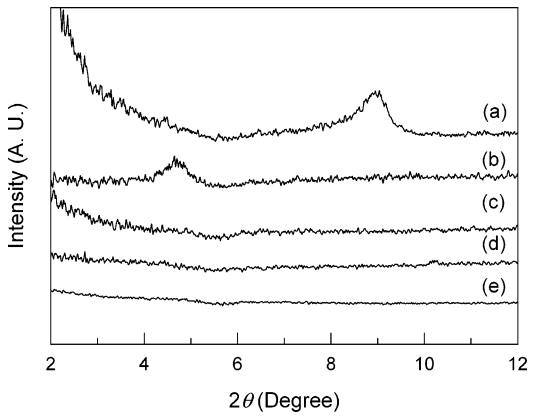

Figure 3. XRD patterns of (a) Na^+-MMT, (b) P(SSNa-*co*-BOC-AMS)/clay nanocomposite, (c) P(SSA-*co*-AMS)/clay nanocomposite, (d) in-situ PSSA-*g*-PANI/clay nanocomposite, and (e) simple blending of PSSA-*g*-PANI and clay.

X-ray diffraction (XRD) has often been used for determining the degree of intercalation and/or exfoliation of clay in the polymer matrix. When XRD patterns for pristine clay (Na^+−MMT), P(SSNa-*co*-BOC-AMS)/clay, P(SSA-*co*-AMS)/clay, in-situ composite of PSSA-*g*-PANI/clay, and simple blending of PSSA-*g*-PANI and clay are compared with each other, as shown in Figure 3, the following facts are realized. First, the *d*-spacing of Na^+−MMT in P(SSNa-*co*-BOC-AMS)/clay increases from 9.8 Å in pristine clay to 19.4 Å, as shown in Figure 3a and b, indicating that P(SSNa-*co*-BOC-AMS) chains are intercalated into the gallery of clay layers. The

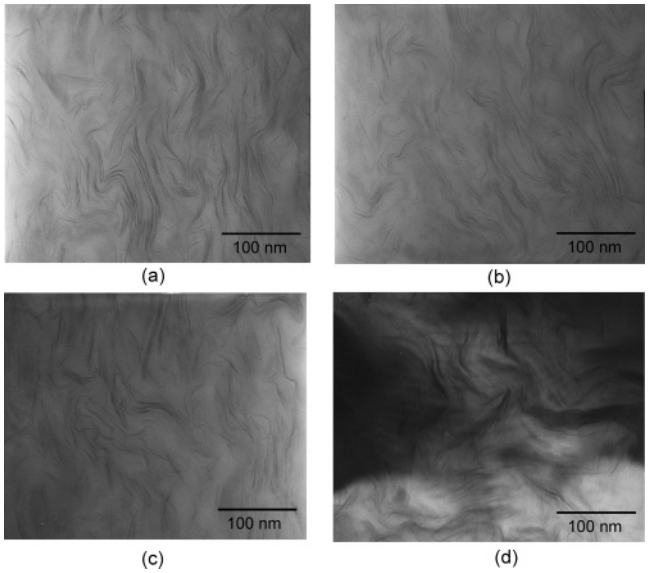

Figure 4. TEM images of (a) in-situ PSSA-*g*-PANI/clay nanocomposite, (b) simple blending of PSSA-*g*-PANI and clay, (c) P(SSA-*co*-AMS)/clay nanocomposite, and (d) P(SSNa-*co*-BOC-AMS)/clay nanocomposite.

increase of ca. 10 Å in *d*-spacing corresponds roughly to intercalation of one or two polymer chains into each gallery of clay layers. Second, P(SSA-*co*-AMS)/clay does not show any discernible peak in the XRD pattern (Figure 3c), indicating that most of clay layers are exfoliated in the polymer matrix. Since P(SSA-*co*-AMS) obtained after elimination of BOC group from P(SSNa-*co*-BOC-AMS) in acidic aqueous media has positively charged nitrogens (NH_3^+) in its structure, it is expected that an ionic interaction between positively charged nitrogen in P(SSA-*co*-AMS) and the negatively charged surface of clay layers attributes to exfoliation of clay layers in the polymer matrix. Third, in-situ composite of PSSA-*g*-PANI/clay shows an exfoliated structure, as can be seen in Figure 3d. This indicates that the exfoliated structure of P(SSA-*co*-AMS)/clay is preserved while in-situ composite of PSSA-*g*-PANI/clay is prepared by in-situ graft copolymerization of ANI onto P(SSA-*co*-AMS)/clay. Here, it is noteworthy that the protonated imine nitrogen in grafted PANI is more favorable to interact with negatively charged surface of clay layers than the positively charged nitrogen in P(SSA-*co*-AMS). Finally, simple blending of water-soluble PSSA-*g*-PANI and Na^+−MMT also yields exfoliated structure, as shown in Figure 3e.

To more clearly identify exfoliated structures of the nanocomposites, we obtained TEM images of the composites, as shown in Figure 4, where dark stripes represent the clay layers and the gray/white area represents the polymer matrix. TEM images of in-situ composite of PSSA-*g*-PANI/clay (Figure 4a), simple blending of PSSA-*g*-PANI and clay (Figure 4b), and P(SSA-*co*-AMS)/clay (Figure 4c) show fully exfoliated structures, i.e., the nanosized clay sheets are uniformly dispersed in the polymer matrix. On the other hand, the TEM image of P(SSNa-*co*-BOC-AMS)/clay (Figure 4d) shows that the composite has a considerable amount of stacked layers in which polymer chains are intercalated, which is consistent with the result of X-ray diffraction (Figure 3b).

When the C−N stretching vibration in the FTIR spectrum of PSSA-*g*-PANI is compared with that of PSSA-*g*-PANI/clay nanocomposite, it is revealed that the C−N stretching vibration of in-situ PSSA-*g*- PANI/clay nanocomposite at 1303 cm^{-1} is slightly higher than that of PSSA-*g*-PANI at 1301 cm^{-1}, as shown in Figure 5a. This is probably due to physical interaction between PANI chain and silicate layers.[14,15] Another important feature to be noted from Figure 5a is that the peak of PSSA-*g*-PANI at 1216 cm^{-1}, as interpreted as $C-N^+$ stretching vibration in the polaron structure, not only shifts to higher frequency (1230 cm^{-1}) but also becomes stronger in intensity when PSSA-*g*-PANI/clay nanocomposite is prepared. This indicates that the Coulombic interaction between the positive nitrogen of PSSA-*g*-PANI and the negatively charged surface of clay layers affects the vibrational motion of PANI.[19] When the C−N stretching vibration of P(SSNa-*co*-BOC-AMS) is compared with that of P(SSNa-*co*-BOC-AMS)/clay, it is revealed that the C−N vibration peak of P(SSNa-*co*-BOC-AMS) at 1317 cm^{-1} does not change, as shown in Figure 5b. This is because P(SSNa-*co*-BOC-AMS) does not have positive charges for ionic interaction with the negatively charged surface of clay. Figure 5c shows that the C−N vibration peak of P(SSA-*co*-AMS) shifts to higher frequency by 4 cm^{-1} when P(SSA-*co*-AMS) forms the nanocomposite with clay. This is because P(SSA-*co*-AMS) has positively charged nitrogens (NH_3^+) for interaction with the negatively charged surface of clay layer.

The UV−vis spectrum of in-situ PSSA-*g*-PANI/clay nanocomposite (or simple blending of PSSA-*g*-PANI and clay) shows that polaron band transitions take place at 418 and 801 nm (or 417 and 797 nm), as shown in Figure 6b and c, indicating that both PSSA-*g*-PANI/clay

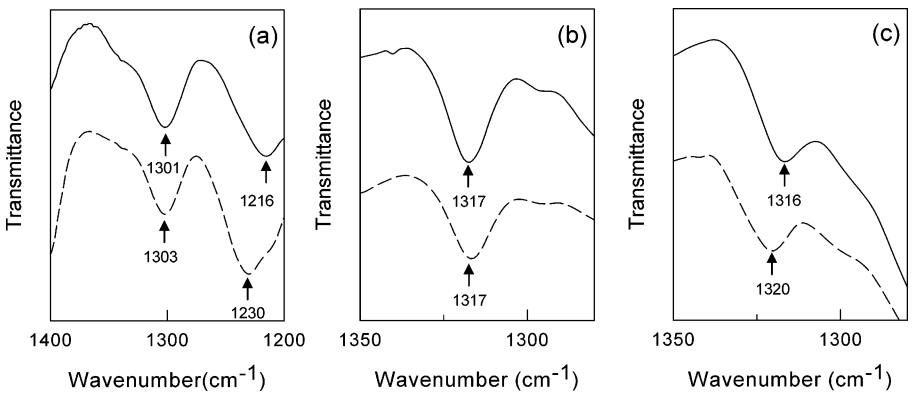

Figure 5. Comparison of C−N stretching vibration bands: (a) PSSA-*g*-PANI versus in-situ PSSA-*g*-PANI/clay nanocomposite, (b) P(SSNa-*co*-BOC-AMS) versus P(SSNa-*co*-BOC-AMS)/clay nanocomposite, and (c) P(SSA-*co*-AMS) and P(SSA-*co*-AMS)/clay nanocomposite. Solid line and dashed line represent pure polymer and polymer/clay nanocomposite, respectively.

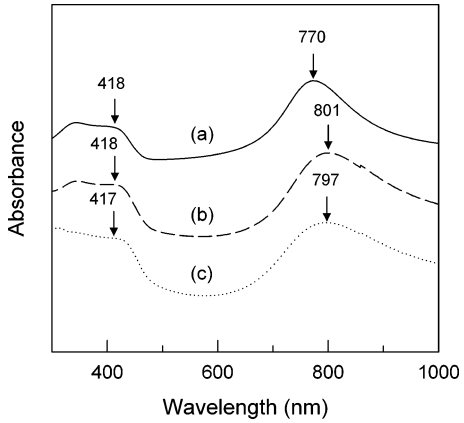

Figure 6. UV−vis spectra of (a) PSSA-*g*-PANI, (b) in-situ PSSA-*g*-PANI/clay nanocomposite, and (c) simple blending of PSSA-*g*-PANI and clay.

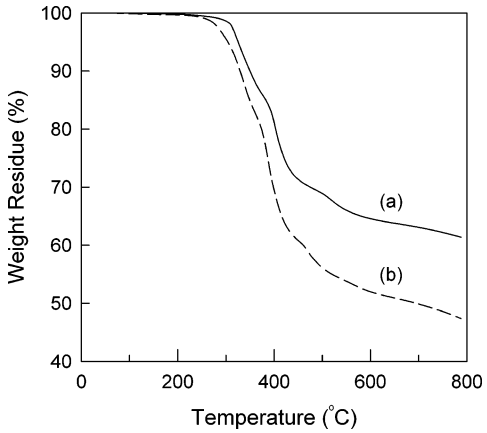

Figure 7. TGA curves of (a) in-situ PSSA-*g*-PANI/clay nanocomposite and (b) PSSA-*g*-PANI.

nanocomposites are in a conducting state. The peak at 770 nm for PSSA-*g*-PANI shifts to 797 and 801 nm for in-situ PSSA-*g*-PANI/clay nanocomposite and simple blending of PSSA-*g*-PANI and clay, respectively. This shifting of the peak to higher wavelength indicates an increase of conjugation length, a decrease of band gap energy, and a delocalization of electrons in the polaron band.[20] This is attributed to the more extended chain conformation of PSSA-*g*-PANI in PSSA-*g*-PANI/clay nanocomposite as compared to the pure PSSA-*g*-PANI. The exfoliated layers of Na^+−MMT may interact with PSSA-*g*-PANI, and the interaction makes the polymer chains more extended. As a result, the polaron band becomes more dispersed in energy.[12]

Although the polaron band transition peak of PANI in PSSA-*g*-PANI/clay nanocomposites shifts to higher wavelength as compared to that of pure PSSA-*g*-PANI, the electrical conductivities of in-situ PSSA-*g*-PANI/clay nanocomposite and simple blending of PSSA-*g*-PANI and clay were 4.7×10^{-2} and 4.2×10^{-2} S/cm, respectively, which are lower than the conductivity of PSSA-*g*-PANI (1.2×10^{-1} S/cm). This decrease of conductivity is attributed to interruption of interchain hopping of charges between PSSA-*g*-PANI chains by uniformly dispersed clay sheets. However, the decrease is not so significant considering that the nanocomposites contain a large content of clay (13 wt %). Here, it should be mentioned that the electrical conductivity of intercalated PANI/clay nanocomposite is reported to decrease by at least 2 orders of magnitude as compared to PANI by other workers.[20]

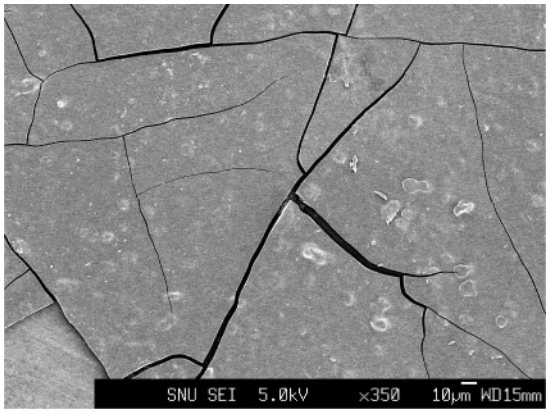

(a)

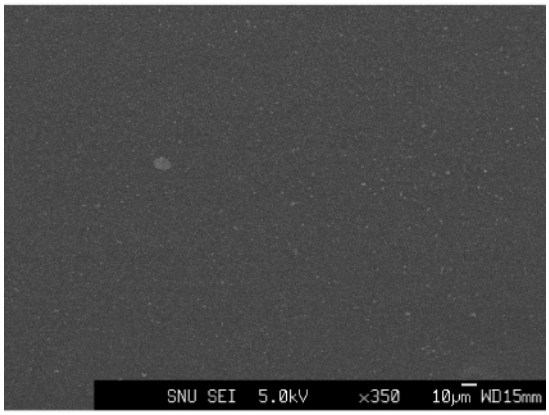

(b)

Figure 8. FESEM images of (a) PSSA-*g*-PANI and (b) PSSA-*g*-PANI/clay nanocomposite spin-coated on silicon wafer.

Figure 7 compares the thermal stability of the PSSA-*g*-PANI/clay nanocomposite with that of the PSSA-*g*-PANI. Both PSSA-*g*-PANI and in-situ PSSA-*g*-PANI/clay nanocomposite do not show any significant weight loss up to 300 °C in the TGA curve, whereas the PANIs doped with acid dopants are reported to decompose at 200−300 °C.[21] The better thermal stability of our system is probably because the polymeric dopant (backbone PSSA) in our system is covalently bonded to PANI. The weight loss starting at around 300 °C is attributed to elimination of sulfonic acid groups, which is mostly accompanied with evolution of SO_2 as reported by Gupta and Scherer[22] and Hietala et al.[23] It was also reported that the thermal decompositions starting at around 400 and 500 °C are attributed to the decomposition of PSSA and PANI, respectievely.[24,25] When the TGA curve of in-situ PSSA-*g*-PANI/clay nanocomposite is compared with that of PSSA-*g*-PANI, as shown in Figure 7, it is revealed that in-situ nanocomposite is thermally more stable than that of PSSA-*g*-PANI. This is probably because the attractive Coulombic interaction between the positive nitrogen in PSSA-*g*-PANI and the negatively charged surface of the clay layer improves the thermal stability.

When the surface morphology of a spin-coated film of PSSA-*g*-PANI/clay nanocomposite was compared with that of PSSA-*g*-PANI, it is observed that the nanocomposite has a better coatability than PSSA-*g*-PANI, as shown in Figure 8. The film of PSSA-*g*-PANI coated on glass plate or silicon wafer shows surface cracks (Figure

8a), while the film of PSSA-*g*-PANI/clay nanocomposite has a very uniform surface (Figure 8b). This is because the clay layers are dispersed in the polymer matrix on the nanoscale and therefore effectively reinforce the polymer matrix.

Conclusions

Exfoliated PSSA-*g*-PANI/clay nanocomposites have been successfully prepared by in-situ graft polymerization of ANI onto pre-exfoliated P(SSA-*co*-AMS)/clay nanocomposite or by simple blending of PSSA-*g*-PANI and Na^+−MMT. XRD patterns and TEM images clearly show exfoliation of clay layers in the polymer matrix on the nanoscale. Analysis of FTIR spectra reveals that the Coulombic interaction between the positive nitrogen in the polymer and the negatively charged surface of the clay plays an important role in exfoliation of clays in the polymer matrix. The electrical conductivity of PSSA-*g*-PANI/clay nanocomposite (4.7×10^{-2} S/cm) is slightly lower than that of pure PSSA-*g*-PANI (1.2×10^{-1} S/cm). However, this drop of conductivity is not as significant as the case of intercalated PANI/clay nanocomposite. It is observed that the PSSA-*g*-PANI/clay nanocomposite has better thermal stability and better coatability than PSSA-*g*-PANI.

Acknowledgment. The authors thank the Korea Science and Engineering Foundation (KOSEF) for financial support through the Hyperstructured Organic Materials Research Center (HOMRC).

References and Notes

(1) Gustafasson, G.; Cao, Y.; Heeger, J. *Nature* **1992**, *357*, 478.
(2) In *Handbook of Conducting Polymers*, 2nd ed.; Skotheim, T. A., Elsenbaumer, R. L., Reynolds, J. F., Eds.; Marcel Dekker: New York, 1998.
(3) In *Handbook of Organic Conductive Molecules and Polymers*; Nalwa, H. S., Ed.; John Wiley & Sons Inc.: Chichester, 1997.
(4) Wang, X. H.; Li, J.; Zhang, J. Y.; Sun, Z. C.; Yu, L.; Jing, X. B.; Wang, F. S.; Sun, Z. X.; Ye, Z. J. *Synth. Met.* **1999**, *102*, 1224.
(5) Focke, W. W.; Wnek, G. E.; Wei, Y. *J. Phys. Chem.* **1987**, *91*, 5813.
(6) Kingsborough, R. P.; Swager, T. M. *Adv. Mater.* **1998**, *10*, 1100.
(7) Ruiz-Hitzky, E.; Aranda, P.; Casal, B.; Galván, J. C. *Adv. Mater.* **1995**, *7*, 180.
(8) Allcock, H. R. *Science* **1992**, *255*, 1106.
(9) Giannelis, E. P. *Adv. Mater.* **1996**, *8*, 29.
(10) Leroux, F.; Goward, G.; Power, W. P.; Nazar, L. F. *J. Electrochem. Soc.* **1997**, *144*, 3886.
(11) Kerr, T. A.; Wu, H.; Nazar, L. F. *Chem. Mater.* **1996**, *8*, 2005.
(12) Wu, Q.; Xue, Z.; Qi, Z.; Wang, F. *Polymer* **2000**, *41*, 2029.
(13) Nascimento, G. M.; Constantino, V. R. I.; Temperini, M. L. A. *Macromolecules* **2002**, *35*, 7535.
(14) Kim, J. W.; Kim, S. G.; Choi, H. J.; Jhon, M. S. *Macromol. Rapid Commun.* **1999**, *20*, 450.
(15) Kim, B. H.; Jung, J. H.; Hong, S. H.; Joo, J. S.; Epstein, A. J.; Mizoguchi, K.; Kim, J. W.; Choi, H. J. *Macromolecules* **2002**, *35*, 1419.
(16) Yeh, J. M.; Liou, S. J.; Lai, C. Y.; Wu, P. C. *Chem. Mater.* **2001**, *13*, 1131.
(17) Bae, W. J.; Kim, K. H.; Park, Y. H.; Jo, W. H. *Chem. Commun.* **2003**, *22*, 2769.
(18) Park, Y. H.; Cheung, J. S. *J. Korean Fiber Soc.* **1989**, *26*, 65.
(19) Stutzmann, T.; Siffert, B. *Clay Clay Miner.* **1977**, *25*, 392.
(20) Ioune, H.; Yoneyama, H. *J. Electroanal. Chem.* **1987**, *233*, 291.
(21) Lee, D.; Char, K. *Polym. Degrad. Stabil.* **2002**, *75*, 555.
(22) Gupta, B.; Scherer, G. G. *J. Appl. Polym. Sci.* **1993**, *50*, 2129.
(23) Hietala, S.; Keol, M.; Elomaa, M.; Sundholm, F. *J. Mater. Chem.* **1998**, *11*, 327.
(24) Hietala, S.; Koel, M.; Skou, E.; Elomaa, M.; Sundholm, F. *J. Mater. Chem.* **1998**, *8*, 1127.
(25) Ding, L.; Wang, X.; Gregory, R. V. *Synth. Met.* **1999**, *104*, 73.

MA048829B